doi:10.1016/j.jmb.2008.10.091 J. Mol. Biol. (2009) 385, 1003–1013

JMB

Available online at www.sciencedirect.com

ScienceDirect

ELSEVIER

Binding Hot Spot in the Weak Protein Complex of Physiological Redox Partners Yeast Cytochrome *c* and Cytochrome *c* Peroxidase

Alexander N. Volkov, Qamar Bashir, Jonathan A. R. Worrall and Marcellus Ubbink*

Gorlaeus Laboratories, Leiden Institute of Chemistry, Leiden University, PO Box 9502, 2300 RA Leiden, The Netherlands

Received 29 August 2008; received in revised form 16 October 2008; accepted 30 October 2008
Available online 8 November 2008

Transient protein interactions mediate many vital cellular processes such as signal transduction or intermolecular electron transfer. However, due to difficulties associated with their structural characterization, little is known about the principles governing recognition and binding in weak transient protein complexes. In particular, it has not been well established whether binding hot spots, which are frequently found in strong static complexes, also govern transient protein interactions. To address this issue, we have investigated an electron transfer complex of physiological partners from yeast: yeast *iso*-1-cytochrome *c* (Cc) and yeast cytochrome *c* peroxidase (CcP). Using isothermal titration calorimetry and NMR spectroscopy, we show that Cc R13 is a hot-spot residue, as R13A mutation has a strong destabilizing effect on binding. Furthermore, we employ a double-mutant cycle to illustrate that Cc R13 interacts with CcP Y39. The present results, in combination with those of earlier mutational studies, have enabled us to outline the extent of the energetically important Cc–CcP binding region. Based on our analysis, we propose that binding energy hot spots, which are prevalent in static protein complexes, could also govern transient protein interactions.

Keywords: NMR spectroscopy; isothermal titration calorimetry; double-mutant cycles; protein–protein interactions; transient complex

Edited by J. E. Ladbury

Introduction

Interactions between proteins mediate most cellular functions. The variation in the strengths of protein–protein complexes is staggering—the corresponding dissociation constants span a range of 12 orders of magnitude.[1] At one extreme of this continuum are tight (nanomolar to subpicomolar), long-lived, highly specific complexes (e.g., those of antigens and antibodies, or enzymes and inhibitors), which we refer to as "static" in this work. At the other end of the scale are weak (millimolar to micromolar) short-lived complexes formed by proteins that recognize multiple partners. These interactions, referred to as "transient," orchestrate biochemical transmission processes such as those taking place in signal transduction cascades or electron transfer (ET) chains.

Despite their functional importance and because of difficulties associated with their structural characterization, weak transient complexes are largely underrepresented in published analyses of protein interfaces.[2–7] As a consequence, the present understanding of the principles underlying protein–protein recognition and binding comes almost exclusively from the study of static complexes. It has been shown that many factors that are believed to determine binding strength in static complexes

*Corresponding author. E-mail address: m.ubbink@chem.leidenuniv.nl.

Present addresses: A. N. Volkov, Department of Biochemistry, 117 Schweitzer Hall, University of Missouri-Columbia, Columbia, MO 65211, USA; J. A. R. Worrall, Department of Biological Sciences, University of Essex, Wivenhoe Park, Colchester CO4 3SQ, UK.

Abbreviations used: Cc, yeast *iso*-1-cytochrome *c*; CcP, yeast cytochrome *c* peroxidase; ET, electron transfer; SASA, solvent-accessible surface area; ITC, isothermal titration calorimetry; wt, wild type; 1D, one-dimensional; 2D, two-dimensional; HSQC, heteronuclear single quantum coherence; 3D, three-dimensional; PDB, Protein Data Bank.

(such as shape complementarity, interface size, and specific intermolecular contacts) are much less important for transient ones.[8,9] This raises a question of how much of what we have learned from static complexes holds true for their transient counterparts. In particular, it would be interesting to know whether binding hot spots, which are frequently found in static complexes,[4,7,10–12] also govern transient protein interactions.

In a seminal alanine scanning mutagenesis study of human growth hormone binding to its receptor, Clackson and Wells showed that only a few surface residues on both proteins are energetically important for the interaction.[13] These are clustered together in an interface region, aptly named "hot spot," and surrounded by residues whose replacement by alanine has a small or no effect on binding energy. A further analysis of hot spots in protein–protein complexes has shown that, as a rule, those are located in the center of the interface and enriched in tryptophan, tyrosine, and arginine groups.[4] Furthermore, it was demonstrated that hot-spot residues—defined as those increasing the binding free energy of the complex by ≥ 2 kcal mol^{-1} upon mutation to alanine—constitute on average only ~10% of all interfacial residues.[7] At present, it is not clear whether binding hot spots orchestrate transient protein interactions; to the best of our knowledge, these have been reported for only one weak complex ($K_d \sim 2$ μM).[14] Interestingly, analysis of transient ET protein complexes reveals that their binding site architecture is highly suitable for hot spots, with an enhanced hydrophobic environment at the center of the interface, charged residues at the periphery, and interface enrichment in arginine residues.[9]

Despite having been extensively studied in the past several decades, the yeast *iso*-1-cytochrome *c* (Cc)–yeast cytochrome *c* peroxidase (CcP) complex remains a popular system for the investigation of biomolecular ET.[15,16] The Cc–CcP crystal structure has been solved,[17] and a paramagnetic relaxation enhancement NMR study has established that the protein–protein orientation observed in the crystal is indeed the dominant form of the complex in solution.[18] This result confirmed the findings of an earlier NMR chemical shift perturbation mapping, which showed that Cc binding site in solution is very similar to that observed with X-ray crystallography.[19] Finally, Nakani *et al.* and Pearl *et al.* have demonstrated in a series of recent studies that CcP has a single catalytically active Cc binding domain—the one observed in the X-ray structure of the complex.[20–22]

In the crystal, the Cc–CcP interaction is maintained by multiple van der Waals contacts and a single intermolecular hydrogen bond (Cc N70–CcP E290; Fig. 1a). The small (1150 Å^2) binding interface is formed by residues surrounding the heme group of Cc and located in a surface patch on CcP (Fig. 1b and c). Upon binding, R13 of Cc and Y39 of CcP (Fig. 1b and c, green) lose 67 Å^2 and 107 Å^2 of their solvent-accessible surface areas (SASAs), respectively, which makes them the most buried residues in the interface. Arginine and tyrosine are two of the most frequent hot-spot residues[4] and are commonly found in the binding sites of redox protein complexes.[9]

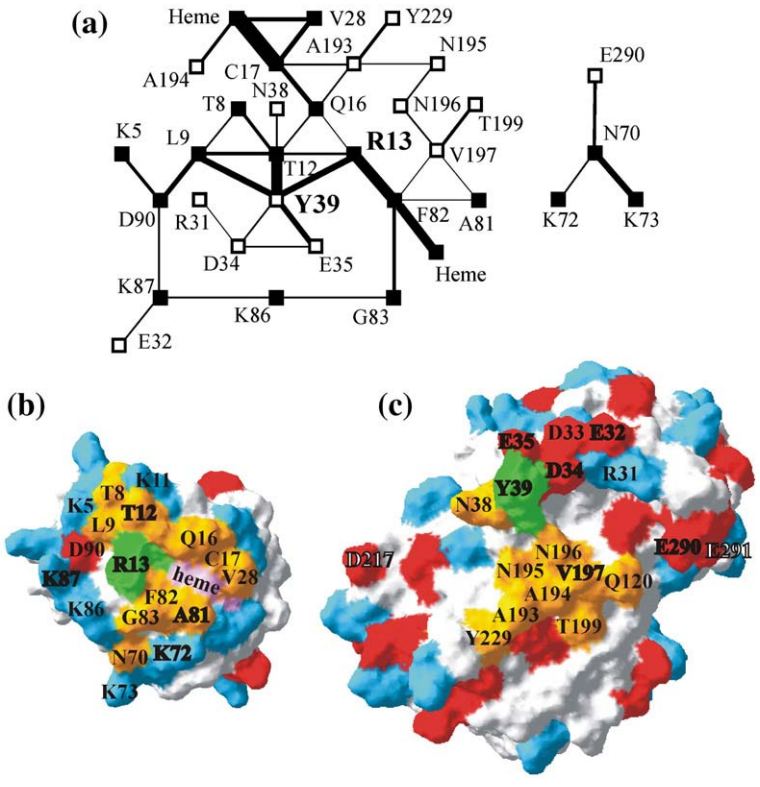

Fig. 1. Cc–CcP binding interface as seen in the crystal structure (PDB entry 2PCC).[17] (a) Cc–CcP contact map. Filled and open squares denote Cc and CcP residues, respectively. The legitimate noncovalent interatomic contacts between interface residues have been identified and analyzed using the CSU software,[23] as described in Materials and Methods. The lengths of the lines connecting the nodes are arbitrary, while their widths denote the strengths of the interactions (see Materials and Methods). Enlarged labels indicate the most buried Cc and CcP residues in the interface: R13 and Y39, respectively. (b and c) Binding surfaces of (b) Cc and (c) CcP. Negatively and positively charged residues are shown in red and blue, respectively. The amino acids that lose SASA upon complex formation are colored and indicated by filled labels. Cc heme group is shown in pink. The two most buried interface residues investigated in this study are shown in green. Bold and open labels identify, respectively, the residues located within and outside of the crystallographically defined binding site, and for which the effects of mutations on K_B are known from this and earlier studies.

Surrounded by a shell of atoms making van der Waals contacts with the partner protein, R13 of Cc sits in the middle of the interface (Fig. 1b). Its central position and a likely occlusion from the solvent make R13 a prime candidate for a binding hot spot in the Cc–CcP complex. Similarly, CcP residue Y39, which makes an intermolecular contact with R13 of Cc (Fig. 1a), could be part of the corresponding hot spot on CcP.

Using isothermal titration calorimetry (ITC) and NMR spectroscopy, we show that R13A mutation of Cc has a strong destabilizing effect on binding ($\Delta\Delta G \geq 2$ kcal mol^{-1}), while the effect of Y39A CcP substitution is a little less pronounced ($\Delta\Delta G =$ 1.6 kcal mol^{-1}). In addition, double-mutant cycle analysis confirms that the Cc R13–CcP Y39 interaction stabilizes the protein complex. Together with the results of earlier mutational studies,[24,25] these findings have enabled us to outline the extent of the energetically important Cc–CcP binding region.

Results

Cc–CcP contact map

Following the work of Reichmann *et al.*, we have constructed the Cc–CcP interaction map[26] (Fig. 1a). In brief, all contacts between the interface residues in the crystal structure of the complex[17] were identified and analyzed (Materials and Methods). Only legitimate[23] noncovalent sequence-specific[26] interatomic contacts below a predefined cutoff distance were selected and weighed according to the type of interaction (see Materials and Methods). Note that backbone–backbone interactions, which are non-sequence-specific,[26] were disregarded. The width of the lines connecting any two nodes in Fig. 1a is proportional to the sum of the weighted interatomic contacts between the two residues. In their study of tight protein complexes, such as TEM-1 β-lactamase inhibitory protein or barnase–barstar complex, Reichmann *et al.* disregarded some of the van der Waals interactions.[26] We, however, have included those in our analysis of the weak transient binding between Cc and CcP, dominated by intermolecular van der Waals contacts.[17] The resulting contact map shows that although both proteins bury equal amounts of SASA upon complex formation (ca 570 Å^2 each), the interactions of Cc side chains are more extensive (Fig. 1a). On the CcP side, most of the interactions are clustered around several residues, one of which (Y39) could make as much as five intermolecular and intramolecular contacts with its interface neighbors (Fig. 1a).

Binding parameters obtained from ITC and NMR

To explore the role of putative hot-spot residues Cc R13 and CcP Y39 in Cc–CcP complex formation, we have studied the binding of R13A Cc and Y39A CcP variants. The binding parameters for the mutant complexes are combined in Table 1. Representative ITC curves for the Cc complexes with wild-type (wt) and Y39A CcP are shown in Fig. 2. All titrations, analyzed with 1:1 and 2:1 binding models, fit best to a 1:1 model, suggesting that no detectable binding of the second Cc takes place under the conditions used. The ITC runs for wt Cc–Y39A CcP are noisy (Fig. 2), giving rise to large errors for the extracted thermodynamic parameters (Table 1). Under the present experimental conditions (see Materials and Methods), the interaction of R13A Cc with either wt CcP or Y39A CcP could not be detected by ITC. The use of higher protein concentrations led to aggregation, precluding ITC analysis of the R13A Cc interaction.

To measure the binding constants for R13A Cc–CcP complexes and to verify the one obtained by ITC for wt Cc–Y39A CcP, we have performed NMR titrations (Fig. 3). In each case, chemical shift perturbations of Cc resonances are followed as Cc is titrated into CcP. As the Cc–CcP complex is in fast exchange on the NMR chemical shift time scale,[19] a single set of

Table 1. Cc–CcP binding parameters

	N[a]	n[b]	K_B[c]	ΔG_B (kcal mol^{-1})	ΔH_B (kcal mol^{-1})	$-T\Delta S_B$ (kcal mol^{-1})
			wt CcP			
wt Cc						
ITC	3	1.05±0.02	19±0.4	−7.3±0.1	−1.6±0.1	−5.7±0.2
NMR[d]	1	1.0	20	−7.3		
R13A						
NMR	1	1.04±0.07	0.6±0.2	−5.2±0.2		
			Y39A CcP			
wt Cc						
ITC	3	1.15±0.07	4±1	−6.4±0.2	−0.7±0.1	−5.7±0.2
NMR	1	1.07±0.03	1.4±0.3	−5.7±0.1		
R13A						
NMR	1	1.0	0.57±0.02	−5.2±0.1		

Experiments were performed in 20 mM sodium phosphate and 0.1 M NaCl (pH 6.0) at 303 K. The uncertainties are the standard errors of the fit for NMR data and the standard deviation of the mean for the ITC experiments.

[a] Number of titrations performed.
[b] Binding stoichiometry.
[c] Equilibrium binding constant: 10^4 M^{-1}.
[d] Lower limit of the binding constant taken from our previous work.[19]

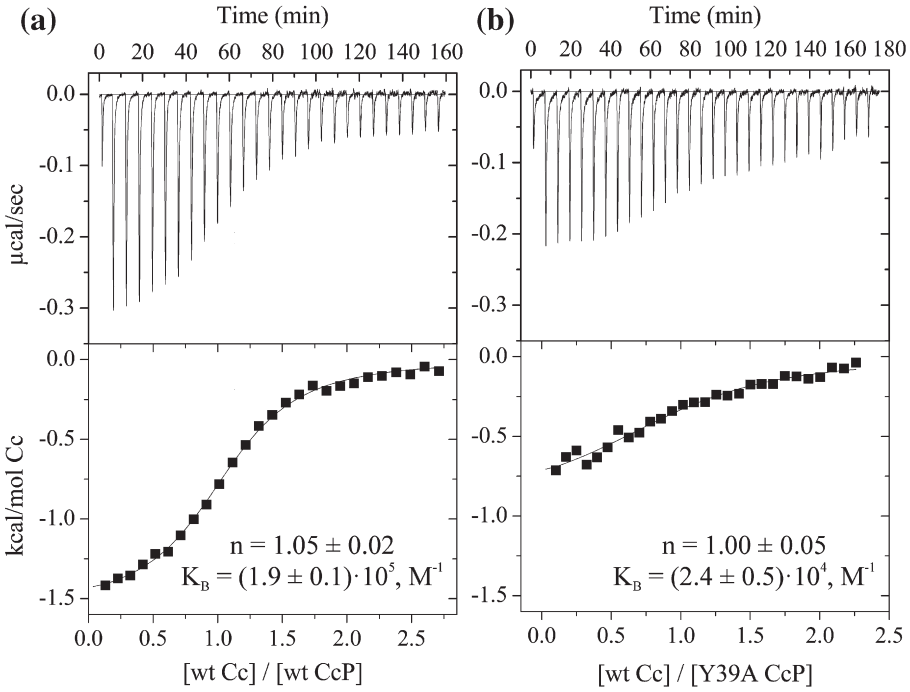

Fig. 2. Representative ITC curves for the binding of wt Cc to (a) wt or (b) Y39A CcP. The top and bottom panels show, respectively, raw data after baseline correction and integrated data corrected for the heat of dilution of Cc. Solid lines in the bottom panels are the best fits to the 1:1 binding model, with the stoichiometry (n) and the binding constants (K_B) indicated. The thermodynamic binding parameters and experimental conditions are given in Table 1. (a) Wt Cc (0.8 mM) was titrated into 0.06 mM wt CcP; (b) 1.5 mM wt Cc and 0.15 mM Y39A CcP were used.

Cc peaks is observed throughout the titration. Binding of wt Cc to Y39A CcP was followed in a series of one-dimensional (1D) ^{1}H NMR spectra by monitoring the changes in the position of a downfield hyperfine-shifted Cc heme resonance (Fig. 3a). For R13A Cc–CcP complexes, chemical shift perturbations of ^{15}N R13A Cc backbone amide resonances were monitored in a series of two-dimensional (2D) [^{1}H,^{15}N] heteronuclear single quantum coherence (HSQC) spectra (Fig. 3b and c). In most cases, the data fitted well to a 1:1 binding model (Eq. (2); Materials and Methods), with the binding constants given in Table 1. For wt Cc–Y39A CcP complex, the K_B value determined by NMR is somewhat lower than that obtained from ITC (Table 1). For the sake of consistency, we have used the K_B values derived from NMR titrations for further analysis of all protein complexes.

Double-mutant cycle

For two interacting proteins, double-mutant cycles allow the identification of pairs of residues whose side chains form stabilizing intermolecular contacts.[27–29] To this end, each residue is substituted by an alanine, and the effects of the mutations on binding are measured. Noncooperativity of the effects of the two mutations (i.e., the change in free energy for the double mutant is the sum of free energies for the two single mutations) indicates that either the two residues do not interact or their interaction does not contribute to the binding energy. But if the effects are coupled (i.e., the change in free energy for the double mutant differs from the sum of free energies for the two single mutants), then the mutated residues must form an intermolecular contact affecting the stability of the protein complex. The coupling energy ($\Delta\Delta G_c$), which is a measure of the cooperativity of interaction,[27] can be computed from Eq. (3) (Materials and Methods).[25,28] Using the NMR binding constants given in Table 1, we have calculated $\Delta\Delta G_c = -1.6 \pm 0.3$ kcal mol^{-1} for the Cc R13–CcP Y39 pair. This value indicates that the interaction between Cc R13 and CcP Y39 stabilizes the complex.

NMR chemical shift perturbations

As mentioned above, the interaction between an isotopically labeled protein and its unlabeled partner can be conveniently followed by heteronuclear 2D NMR spectroscopy. For instance, some of the [^{1}H,^{15}N] HSQC resonances of a ^{15}N-labeled protein will change their positions upon binding to an unlabeled target, which can be used to map the interacting protein surfaces.[30] For the wt Cc–Y39A CcP complex investigated in this study, the binding shifts extrapolated to 100% Cc bound ($\Delta\delta_{avg}$; see Materials and Methods) are plotted in Fig. 4. Overall, the $\Delta\delta_{avg}$ values for the Cc–Y39A CcP are smaller than those for Cc–wt CcP. Despite the decrease in $\Delta\delta_{avg}$, the chemical shift perturbation profiles for the two complexes are very similar (Fig. 4), indicating that the same Cc residues are affected by binding to both wt and Y39A CcP.

Weak transient protein–protein interactions can be conveniently described by a two-step binding model, according to which the dominant single-

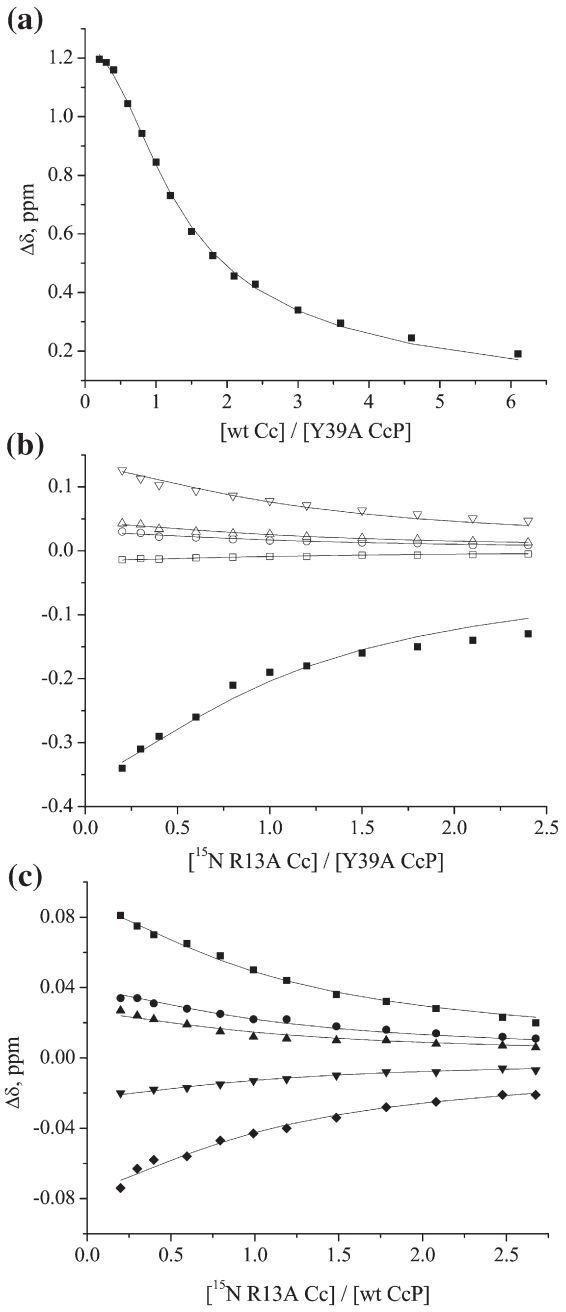

Fig. 3. NMR titrations of (a) wt and (b) R13A Cc with Y39A CcP, and of (c) R13A Cc with wt CcP. (a) Binding shifts of a downfield hyperfine-shifted Cc heme 3-CH_3 resonance followed in 1D ^{1}H NMR spectra. The solid line represents the best fit to a 1:1 binding model. (b and c) Two-dimensional [^{1}H,^{15}N] HSQC binding shifts of the HN (open symbols) and NH (filled symbols) atoms of ^{15}N R13A Cc upon binding to (b) Y39A CcP or (c) wt CcP. The titrations curves are shown for R13A Cc residues: (b) K5 (circles), L9 (triangles), G77 (inverted triangles), and T78 (squares); and (c) A7 (triangles), L9 (squares), T78 (inverted triangles), F82 (diamonds), and D90 (circles). Solid lines in (b) and (c) show the best simultaneous fit of the curves to a 1:1 binding model with a shared K_B value. The obtained binding parameters and experimental conditions are given in Table 1.

orientation complex is in equilibrium with a dynamic encounter state consisting of multiple protein–protein orientations.[8,18,31] As emerges from the study of transient interactions in our group, the reduction in the size of $\Delta\delta_{avg}$ signifies a shift towards the encounter state.[31–35] Thus, the decrease in $\Delta\delta_{avg}$ for Cc–Y39A CcP suggests that the proteins spend more time in search of the dominant binding geometry within this complex.

Interaction of Cc R13 and CcP Y39 side chains

Similarly to backbone amides, $N_\varepsilon H$ groups of arginine side chains give rise to NMR signals in 2D [^{1}H,^{15}N] HSQC experiments. In addition to R13, yeast Cc contains two more arginines (R38 and R91), and the $N_\varepsilon H$ peaks of all three residues are observed in the HSQC spectrum of the wt protein (Fig. 5a). By recording the spectrum of R13A Cc and by comparing it to that of the wt Cc, we were able to unambiguously assign the R13 $N_\varepsilon H$ resonance of the wt protein ($\delta_H = 7.031$ ppm; $\delta_N = 83.09$ ppm).

The R13 side-chain amide of Cc is strongly affected by binding to the wt CcP (Fig. 5a). The chemical shift perturbations extrapolated to 100% form ($\Delta\delta$; see Materials and Methods) are 0.704 ppm and 0.96 ppm for the $N_\varepsilon H$ proton and nitrogen, respectively. At the same time, interaction with Y39A CcP results in smaller binding shifts ($\Delta\delta_H = 0.148$ ppm; $\Delta\delta_N = 0.82$ ppm). The difference in the size of $\Delta\delta$ upon binding to wt and Y39A CcP is especially prominent along the proton dimension (Fig. 5a), with $\Delta\Delta\delta_H = \Delta\delta_H(\text{Cc–wt CcP}) - \Delta\delta_H(\text{Cc–Y39A CcP}) = 0.556$ ppm. Inspection of the crystal structure of the wt complex fails to reveal a structural cause for such a large difference in binding shifts. As can be seen from Fig. 5b, the $N_\varepsilon H$ group of Cc R13 is too far from the CcP surface to either make a direct intermolecular contact or experience a significant ring current effect exerted by the aromatic ring of CcP Y39. Indeed, the ring current shift for the R13 $N_\varepsilon H$ proton calculated from the crystallographic side-chain coordinates is close to zero (−0.048 ppm and −0.074 ppm for the two complexes present in the asymmetric unit; see Materials and Methods). The large $\Delta\delta$ values observed for Cc R13 $N_\varepsilon H$ upon interaction with wt, but not with Y39A CcP, most likely reflect a difference in the binding-induced solvation changes of the Cc R13 group in the two complexes.

Discussion

Cc–CcP binding hot spot

The architecture of the Cc–CcP interface satisfies several important requirements for binding hot spots. On the Cc side, the contact surface is composed of a central core, surrounded by a ring of lysines (Fig. 1b). The observed enhanced hydrophobic environment of the central patch and the presence of an arginine side chain (R13) in the middle of

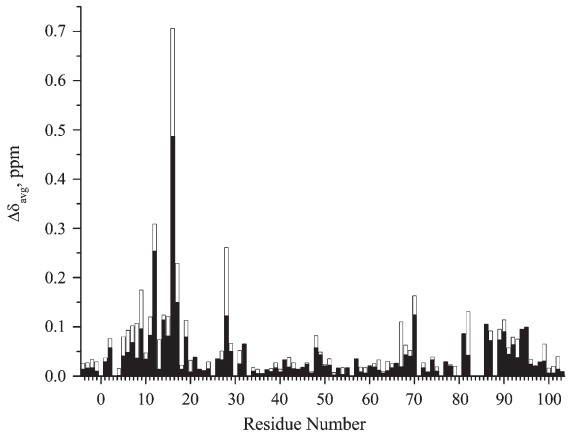

Fig. 4. Chemical shift perturbation analysis of the wt Cc–Y39A CcP complex in solution. Filled and open bars show $\Delta\delta_{avg}$ for the binding of wt Cc to Y39A and wt CcP, respectively, at 303 K in 20 mM sodium phosphate and 0.1 M NaCl (pH 6.0). The values of $\Delta\delta_{avg}$ are extrapolated to 100% bound form (see Materials and Methods).

the binding surface are common features of both redox protein complexes[9] and binding hot spots.[4,7] On the CcP side, the interface consists of two patches located around A194 and D34, and is composed of predominantly hydrophobic and negatively charged amino acids, respectively (Fig. 1c). Joining the two patches is a tyrosine group (Y39)—yet another ubiquitous hot-spot residue.[4,7] Also for the CcP interface, the presence of the hydrophobic core and a polar periphery seems to favor a binding hot spot.

Cc R13 and CcP Y39 are the two most buried amino acids in the interface and are likely the binding anchors[38] in the Cc–CcP complex. As we have shown above, substitution of either CcP Y39 or Cc R13 by an alanine leads to the weakening of the Cc–CcP interaction. While the former results in a moderate change in binding energy ($\Delta\Delta G_B = 1.6$ kcal mol^{-1}), the latter has a larger destabilizing effect on the complex ($\Delta\Delta G_B = 2.1$ kcal mol^{-1}). Thus, our results show that R13 of Cc is indeed a hot-spot residue.

As a rule, hot-spot regions of interacting proteins are complementary (i.e., the binding hot spot on one protein packs against that on the other).[4,7,13] In this regard, the moderate effect of Y39A CcP mutation—which abolishes the interaction with Cc R13 and eliminates weak van der Waals contacts with Cc L9 and T12 (Fig. 1a)—is somewhat puzzling. One explanation for this behavior could be a structural rearrangement in the Cc–Y39A CcP complex. Unfortunately, due to weak binding and increased dynamics, solving the Cc–Y39A CcP structure by X-ray crystallography is a challenging task. Furthermore, paramagnetic relaxation enhancement NMR spectroscopy, which was applied successfully to the wt complex,[18] cannot be used to elucidate the solution structure of such highly dynamic protein–protein system because the paramagnetic effects arising from the well-defined form and the highly populated dynamic state of the complex can no longer be separated.[39] However, the similarity of the chemical shift perturbation profiles for Cc bound to wt and Y39A CcP suggests that the latter mutation does not perturb the overall structure of the protein complex. Rather, it seems more likely that slight reorientation of the Cc R13 side chain brings it into contact with other neighboring CcP residues (e.g., D34 or N196; see Fig. 1c), thereby counterbalancing the destabilizing effect of Y39A substitution. Alternatively, the space vacated by the CcP Y39 side chain can now be occupied by one or more water molecules whose interaction with Cc R13 could restore binding.

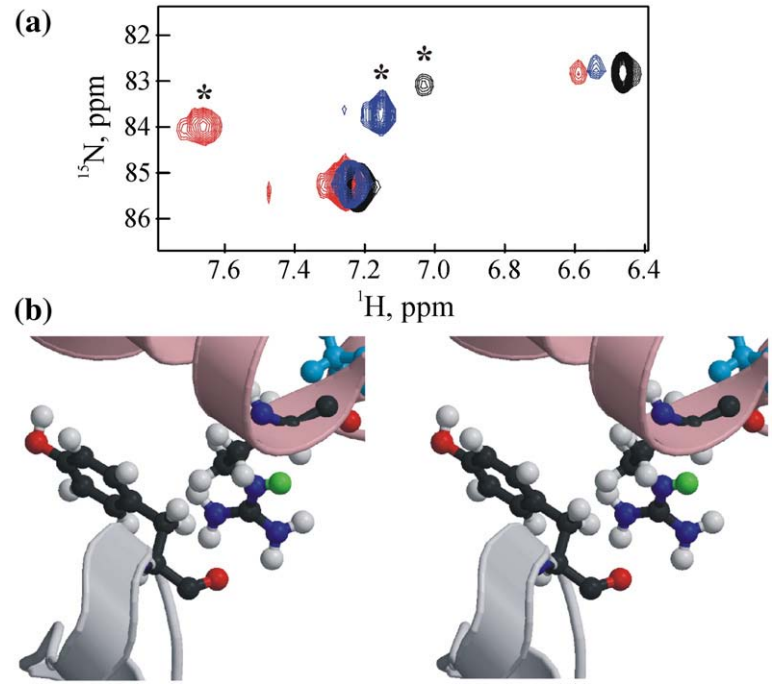

Fig. 5. The interaction between Cc R13 and CcP Y39. (a) Two-dimensional [^{1}H,^{15}N] HSQC resonances of $N_\varepsilon H$ arginine groups of ^{15}N Cc free (black) and in complex with wt CcP (red) or Y39A CcP (blue). Asterisks indicate R13 $N_\varepsilon H$ peaks. (b) Stereo view of Cc R13 and CcP Y39 side chains as seen in the crystal structure of the complex (PDB entry 2PCC). The ribbon representations of Cc and CcP are shown in magenta and gray, respectively. Part of the Cc loop comprising residues 82–87 has been removed for clarity. The Cc heme group (cyan) and the side chains in question are shown in ball-and-sticks representation. The added hydrogen atoms are shown as light-gray spheres, and Cc R13 $N_\varepsilon H$ proton is shown in green. The image in (b) was made with MOLSCRIPT[36] and Raster3D.[37]

In order to define hot-spot regions on the Cc–CcP interface, we have combined our data with those of previous mutagenesis studies (Table 2).[24,25] CcP is known to bind Cc at more than one site; however, at the high ionic strength used in this study (I=125 mM), interactions at alternative sites will be negligible.[15,16] Therefore, in our analysis, we consider mutations of only those CcP residues that are located in or around the crystallographic binding site and for which changes in the binding energy have been reported (Fig. 1c, bold and open labels). As can be seen from Table 2, in addition to Cc R13, there appear to be two other hot-spot residues: Cc A81 and CcP V197. Although $\Delta\Delta G_B$ for an unconventional A81G Cc mutation is slightly below the 2-kcal mol^{-1} threshold, we tentatively classify A81 as part of a hot spot in the transient Cc–CcP complex.

It should be noted that the traditional hot-spot cutoff $\Delta\Delta G_B$=2 kcal mol^{-1} originates from analyses of strong protein interactions[4–7] and constitutes only a small fraction of the total binding energy in tight static complexes (e.g., 12–16% for systems with K_d in the picomolar to nanomolar range). For weak transient interactions, this fraction will be larger (e.g., 27% for the protein complex studied here). If, correspondingly, the cutoff value for Cc–CcP analysis is decreased to 1–1.5 kcal mol^{-1}, the binding hot spot will also include CcP Y39 (Table 2).

Given the location of two energetically important Cc residues (R13 and A81; Fig. 1b), it appears that the Cc hot spot encompasses the region around the heme group. We suggest that other heme neighbors—such as Q16, V28, and F82, which would be prime targets for further mutagenesis—could also be part of the hot spot. Similarly, the residues surrounding the energetically important CcP V197 side chain (e.g., A194, N195, N196, and Q120; Fig. 1c) could form the corresponding hot-spot region on the CcP surface. Interestingly, it has been shown recently that Cc residues T12, R13, V28, and A81 form a binding core in complex with cytochrome bc_1 and determine the specificity of the interaction.[40]

Notably, mutations of the peripheral interfacial residues on both Cc (K72 and K87) and CcP (E32, D34, and E35) have very little influence on protein binding (Table 2 and Fig. 1b and c). Likewise, alanine substitutions of CcP amino acids located outside of the binding interface (Fig. 1c, open labels) have no effect on the complex formation, confirming that the binding geometry observed in the crystal structure persists in the solution complex. Taken at face value, our findings support the O-ring hypothesis, which predicts the energetic unimportance of the side-chain groups surrounding the hot spot.[4] At the same time, the O-ring residues are believed to seal the binding surface from the solvent;[4] however, the Cc–CcP interface is "wet"[17,41]—a situation observed for many protein complexes.[40–43] Thus, it appears that the proposed function of the O-ring might not be universal. An alternative explanation for the neutral effect of alanine mutations of peripheral residues on binding energy is that the side-chain atoms are replaced by water molecules, and that the newly introduced protein–solvent interactions restore binding.[11,42]

To verify our present experimental analysis and to facilitate further study of the Cc–CcP binding hot spot, we have used Robetta[44,45] and ISIS[46]—two web-based computer programs used for predicting hot spots in protein complexes. While the former uses the three-dimensional (3D) structure of a complex and outputs a list of the putative hot-spot residues (together with the predicted $\Delta\Delta G_B$ values for their alanine mutations),[45] the latter predicts binding hot spots from the primary sequence (or, even better, the structure) of an individual protein without prior knowledge of its interaction partner.[46] With the Cc–CcP crystal structure as input and with the recommended cutoff value for the change in binding energy (see Materials and Methods), Robetta identified CcP Y39 and Cc Q16 as two hot-spot residues. Two other energetically important nonalanine side chains discussed in this work (Cc R13 and CcP V197) were predicted to have lesser influence on protein binding (see Materials and Methods). Remarkably, using structures of individual proteins as sole input, ISIS correctly identified two of three hot-spot residues (Cc R13 and Cc A81). Similarly to Robetta, it also predicted CcP Y39 and Cc Q16 to be important for protein binding (for a complete list of putative hot-spot residues, see Materials and Methods).

Table 2. Effects of surface mutations on Cc–CcP binding

Cc	$\Delta\Delta G_B$ (kcal mol^{-1})	CcP	$\Delta\Delta G_B$ (kcal mol^{-1})	CcP	$\Delta\Delta G_B$ (kcal mol^{-1})
T12A[a]	−1.3±0.1	E32Q[b]	0.6±0.4	V197A[c]	2.1±0.2
R13A[d]	2.1±0.2	D34A[c]	−0.9±0.7	D217A[c]	0.4±0.2
K72A[c]	0.3±0.2	D34N[b]	0.8±0.4	E290A[c]	6.2±0.2[e]
A81G[c]	1.9±0.4	E35Q[b]	0.7±0.3	E290N[b]	0.9±0.3
K87A[c]	0.9±0.2	Y39A[d]	1.6±0.2	E291N[b]	−0.1±0.3

[a] Unpublished results; experimental conditions are the same as in the present study.
[b] The data, taken from Erman *et al.*, are for the binding of horse Cc (I=50 mM; 298 K, pH 6.0).[24]
[c] Taken from Pielak and Wang (I=82 mM; 298 K, pH 6.0).[25]
[d] This work (I=125 mM; 303 K, pH 6.0).
[e] The reported value is most likely erroneous[16] and is disregarded in our analysis.

Cc R13–CcP Y39 interaction

We have used a double-mutant cycle—an established methodology for the analysis of interprotein interactions[27–29]—to assess the role of the Cc R13–CcP Y39 intermolecular contact in complex formation. The calculated value of coupling energy ($\Delta\Delta G_c = -1.6 \pm 0.3$ kcal mol^{-1}) indicates that the interaction between the two side chains stabilizes the Cc–CcP complex. This finding further supports the importance of the hot-spot residue Cc R13 for protein binding. Analysis of the NMR chemical shift perturbations of the Cc R13 $N_\varepsilon H$ group suggests that the interaction between Cc R13 and CcP Y39 is likely accompanied by binding-induced hydration changes, which are attenuated in complex with Y39A CcP.

Double-mutant cycles had been used before for characterization of intermolecular Cc–CcP interactions.[25] Interestingly, Cc A81 and CcP V197—two residues identified here as part of a binding hot spot—exhibit the largest coupling energy ($\Delta\Delta G_c = -1.9 \pm 0.7$ kcal mol^{-1}), which confirms their importance for protein–protein association. In addition, favorable coupling energies were measured for several residue pairs separated by more than 8 Å in the crystal structure, which was interpreted as evidence for the structural plasticity of the complex.[25]

Concluding Remarks

In this work, we have identified several hot-spot residues in a weak transient complex of Cc and CcP. Although further work is required to accurately delineate the entire hot spot, our present findings and the results of earlier studies[24,25] allow us to outline the energetically important binding regions on both proteins and suggest the most promising residues for future mutational analysis. Based on the results of Kiel *et al.*[14] and our preset data, we would like to propose that binding energy hot spots, which are prevalent in static protein complexes,[4,7,12] can also govern transient protein interactions.

Materials and Methods

Computational analysis

SASAs were calculated with NACCESS.[47] In order to construct the interaction map in Fig. 1a, we have identified and analyzed interatomic contacts in the Cc–CcP crystal structure [Protein Data Bank (PDB) entry 2PCC][17] using the CSU software†.[23] Only legitimate (as defined in Sobolev *et al.*[23]) noncovalent contacts between the interface residues were analyzed. The interface residues were defined as those that lose >0.05 Å^2 of SASA upon complex formation. As the Cc–CcP crystal structure shows two complexes in an asymmetric unit, both of them were analyzed independently. For all interatomic contacts, the average intermolecular distance was calculated from both crystallographic forms. The resulting contacts closer than 3.7 Å for polar–polar bonds or 4.0 Å for hydrophobic and van der Waals interactions were retained for further analysis. At least three residues were required to define an interaction cluster in Fig. 1a. Following Reichmann *et al.*, the backbone:side-chain interactions were assigned a weight of 1, side-chain:side-chain contacts had a weight of 2, and all backbone:backbone contacts were disregarded as non-sequence-specific.[26] In addition, all weak van der Waals interactions (i.e., those for class VI to class VIII residues, as defined by Sobolev *et al.*[23]) were scaled by 1/2. The final weight of the line connecting any two nodes in Fig. 1a is the sum of the number of possible interatomic bonds weighted by their respective factors.

Two web-based software packages, Robetta‡[44,45] and ISIS§,[46] were used to predict Cc–CcP binding hot spots. For analysis with Robetta, we have submitted the crystal structure of the complex (PDB entry 2PCC)[17] and used the cutoff suggested by the authors ($\Delta\Delta G_B = 1$ kcal mol^{-1}) to screen the output file.[45] In this way, Robetta identified CcP Y39 ($\Delta\Delta G_B = 1.3$ kcal mol^{-1}) and Cc Q16 ($\Delta\Delta G_B = 1.0$ kcal mol^{-1}) as the hot-spot residues. The hot-spot groups Cc R13 and CcP V197 were scored with $\Delta\Delta G_B$ values of 0.4 kcal mol^{-1} and 0.8 kcal mol^{-1}, respectively. For analysis with ISIS, coordinates of individual proteins (without the prosthetic groups) were taken from the crystal structure of the complex (PDB entry 2PCC),[17] and the residues with output scores >50 were considered energetically important. The hot spot predicted by ISIS included residues Y39, I40, Y42, R48, Y153, and N184 for CcP, and residues R13, L15, Q16, F36, and A81 for Cc.

Protein preparation

Both native and ^{15}N-labeled wt Cc were expressed in *Escherichia coli* and purified as previously described.[48,49] The wt CcP was isolated from *E. coli* following published procedures.[50] The mutations studied in this work were introduced by site-directed mutagenesis using the Quik Change™ polymerase chain reaction protocol (Stratagene, La Jolla, CA), with the corresponding wt plasmid as template. All constructs were verified by DNA sequencing, and the mutants were expressed and purified analogously to the wt proteins. Throughout the study, we used ferric Cc and high-spin ferric CcP with previously reported purity criteria.[19] Concentrations of Cc and CcP were determined from UV–Vis spectra using $\varepsilon_{410\ nm} = 106.1$ mM^{-1} cm^{-1} and $\varepsilon_{408\ nm} = 98$ mM^{-1} cm^{-1}, respectively.[19]

NMR spectroscopy

We have used 0.8–1.0 mM free ^{15}N wt Cc and 0.5 mM of its 1:1 complexes with wt or Y39A CcP for chemical shift perturbation analysis. To obtain the binding constants by NMR, 0.5 mM wt or Y39A CcP was titrated with a concentrated stock (1.7–2.2 mM) of wt or ^{15}N R13A Cc. All NMR samples contained 20 mM sodium phosphate, 100 mM NaCl (pH 6.0), and 6% D_2O for lock. In addition, the samples used for 1D ^{1}H or 2D [^{15}N,^{1}H]

† http://bip.weizmann.ac.il/oca-bin/lpccsu

‡ http://robetta.bakerlab.org/

§ http://www.rostlab.org/services/isis

HSQC experiments contained, respectively, 0.1 mM 3-(trimethylsilyl)-propionic acid-D4 (sodium salt) or CH_3-$CO^{15}NH_2$ as internal reference. The pH of the samples was adjusted to 6.00±0.05, with small aliquots of 0.1 M HCl or NaOH. Measurements were performed at 303 K on a Bruker DMX600 spectrometer equipped with a TCI-Z-GRAD CryoProbe (Bruker). One-dimensional ^{1}H spectra with a soft presaturation pulse for water suppression were acquired with a spectral width of 70 ppm and 4096 points. Two-dimensional [^{15}N,^{1}H] HSQC spectra with a water-gate pulse[51] for water suppression were obtained with 1024 and 256 points in the direct and indirect dimensions, respectively. For backbone amide experiments, the spectral widths in ^{15}N and ^{1}H dimensions were 42 ppm and 16 ppm, respectively, with a ^{15}N offset of 119 ppm. For observation of the R13 side-chain amide, the spectral width and the offset in ^{15}N dimension were 70 ppm and 113 ppm, respectively.

All data were processed with Azara 2.7 (provided by W. Boucher, Department of Biochemistry, University of Cambridge‖) and analyzed in Ansig for Windows.[52] Assignments of the HSQC spectra of the free and bound ^{15}N wt Cc were taken from a previous report.[19] The HSQC spectrum of ^{15}N R13A Cc—identical with that of ^{15}N wt Cc, except for several resonances of the residues around the mutation site—has been assigned unambiguously using 3D NOESY-HSQC and 3D TOCSY-HSQC experiments. The average amide chemical shift perturbations ($\Delta\delta_{avg}$) were derived from Eq. (1):

$$\Delta\delta_{avg} = \sqrt{\frac{(\Delta\delta_N/5)^2 + \Delta\delta_H^2}{2}} \quad (1)$$

where $\Delta\delta_N$ and $\Delta\delta_H$ are the chemical shift perturbations of the amide nitrogen and proton, respectively. Given the binding constants in Table 1, 90% and 77% wt Cc are bound to wt and Y39A CcP, respectively, at the protein concentrations used in the chemical shift perturbation experiments. In order to obtain $\Delta\delta_{avg}$ extrapolated to the 100% bound form, the respective $\Delta\delta_{avg}$ values were divided by 0.9 or 0.77.

NMR chemical shift titration curves were analyzed with a two-parameter nonlinear least squares fit using a one-site binding model corrected for dilution effect (Eq. (2)):

$$\Delta\delta_{binding} = 0.5\Delta\delta_0\left(A - \sqrt{A^2 - 4/nR}\right) \quad (2)$$

$$A = 1 + 1/nR + \frac{[Cc]_0 + nR[CcP]_0}{nR[Cc]_0[CcP]_0K_B}$$

where $\Delta\delta_{binding}$ is the chemical shift perturbation at a given protein ratio; $\Delta\delta_0$ is the chemical shift perturbation at 100% Cc bound; R is the [Cc]/[CcP] ratio at a given point; n is the deviation from 1:1 stoichiometry; $[Cc]_0$ and $[CcP]_0$ are the concentrations of the protein stock solution used for the titration and the starting solution, respectively; and K_B is the binding constant of the complex. Thus, $\Delta\delta_{binding}$ and R are the dependent and independent variables, respectively, and $\Delta\delta_0$, K_B, and n are the fitted parameters.

‖ ftp://www.bio.cam.ac.uk/pub/azara/

Isothermal titration calorimetry

To prepare protein samples, Cc and CcP were dialyzed in the same beaker against 20 mM sodium phosphate and 0.1 M NaCl (pH 6.0) for 48–72 h with three buffer changes (buffer volume/sample volume ratio, > 500), using Spectra/Por (Spectrum, Rancho Dominguez, CA) dialysis membranes with molecular weight cutoffs of 3500 and 8000 for Cc and CcP, respectively. After dialysis, protein concentrations were determined from optical spectra.

All experiments were performed on a Microcal VP-ITC calorimeter. Wt Cc solutions of 1.0–1.5 mM were placed in a syringe (rotated at 310 rpm during the experiment) and titrated into the sample cell containing 0.10–0.17 mM Y39A CcP. All titrations were performed with an injection volume of 4 μ l for the first titration points, an injection volume of 10 μ l for all subsequent titration points, a 60 s initial equilibration delay, and a 360 s delay between the injections.

The binding isotherms were analyzed with Microcal™ Origin® 5.0. In each case, the first data point was discarded, and the baseline was adjusted manually. The integrated data were corrected for the heat of Cc dilution, either determined by titrating Cc into the buffer or estimated from the last data points of a complete titration by averaging their integrated areas. At the high ionic strength of the solution used in this study, proton release upon complex formation is expected to be insignificant;[53] therefore, its contribution to the overall heat measured in ITC was neglected. All ITC curves, analyzed with 1:1 and 2:1 binding models included in the software package of the manufacturer,[54] fit best to a 1:1 model.

Double-mutant cycles

The coupling energy parameter $\Delta\Delta G_c$ was calculated from experimental binding data (Table 1) using Eq. (3):[25,28]

$$\Delta\Delta G_c = \Delta G_{X,Y} - \Delta G_{X\to A,Y} - \Delta G_{X,Y\to A} + \Delta G_{X\to A,Y\to A} \quad (3)$$

where X and Y represent the wt residues of Cc and CcP, respectively, and A symbolizes a mutation to alanine. Uncertainties were estimated using standard error propagation procedures.

Ring current shifts

The ring current shift (δ_{rc}) of the Cc R13 $N_\varepsilon H$ proton was calculated from Eq. (4):

$$\delta_{rc} = iBG(r) \quad (4)$$

where i is the intensity factor, B is a constant, and $G(r)$ is a geometric factor. The values of $i = 1.24$ and $B = 5.445\times10^{-6}$ Å were taken from the literature,[55] and $G(r)$ was calculated using the Haigh–Mallion model (Eq. (5)):[56]

$$G(r) = \sum_{ij} s_{ij}\left(\frac{1}{r_i^3} + \frac{1}{r_j^3}\right) \quad (5)$$

where r_i and r_j are the distances from ring atoms i and j to the proton, and s_{ij} is the signed area of the triangle formed by atoms i and j and the proton projected onto the plane of the aromatic ring. The sum is over the

bonds of the ring. To calculate the geometric factor, the coordinates of Cc R13 and CcP Y39 side chains were taken from the crystal structure of the complex (PDB entry 2PCC),[17] to which hydrogen atoms had been added in Xplor-NIH.[57] The ring current shifts were calculated for both complexes in the asymmetric unit (protein chains A and B, and protein chains C and D).

Acknowledgements

We thank Prof. T. K. Sixma for access to an ITC machine. This work was supported by the Netherlands Organization for Scientific Research (NWO-CW; grants 700.50.514, 700.52.425, and 98S1010).

References

1. Janin, J. (2000). Kinetics and thermodynamics of protein–protein interactions. In *Protein-protein Recognition* (Kleanthous, C., ed), pp. 1–32, Oxford University Press, New York.
2. Jones, S. & Thornton, J. M. (1996). Principles of protein–protein interactions. *Proc. Natl Acad. Sci. USA*, **93**, 13–20.
3. Tsai, C. J., Lin, S. L., Wolfson, H. J. & Nussinov, R. (1997). Studies of protein–protein interfaces: a statistical analysis of the hydrophobic effect. *Protein Sci.* **6**, 53–64.
4. Bogan, A. A. & Thorn, K. S. (1998). Anatomy of hot spots in protein interfaces. *J. Mol. Biol.* **280**, 1–9.
5. Lo Conte, L., Chothia, C. & Janin, J. (1999). The atomic structure of protein–protein recognition sites. *J. Mol. Biol.* **285**, 2177–2198.
6. Brinda, K. V. & Vishveshwara, S. (2005). Oligomeric protein structure networks: insights into protein–protein interactions. *BMC Bioinf.* **6**, 296.
7. Moreira, I. S., Fernandes, P. A. & Ramos, M. J. (2007). Hot spots—a review of the protein–protein interface determinant amino-acid residues. *Proteins*, **68**, 803–812.
8. Crowley, P. B. & Ubbink, M. (2003). Close encounters of the transient kind: protein interactions in the photosynthetic redox chain investigated by NMR spectroscopy. *Acc. Chem. Res.* **36**, 723–730.
9. Crowley, P. B. & Carrondo, M. A. (2004). The architecture of the binding site in redox protein complexes: implications for fast dissociation. *Proteins*, **55**, 603–612.
10. Ma, B., Wolfson, H. J. & Nussinov, R. (2001). Protein functional epitopes: hot spots, dynamics and combinatorial libraries. *Curr. Opin. Struct. Biol.* **11**, 364–369.
11. DeLano, W. L. (2002). Unraveling hot spots in binding interfaces: progress and challenges. *Curr. Opin. Struct. Biol.* **12**, 14–20.
12. Reichmann, D., Rahat, O., Cohen, M., Neuvrith, H. & Schreiber, G. (2007). The molecular architecture of protein–protein binding sites. *Curr. Opin. Struct. Biol.* **17**, 67–76.
13. Clackson, T. & Wells, J. A. (1995). A hot spot of binding energy in a hormone-receptor interface. *Science*, **267**, 383–386.
14. Kiel, C., Selzer, T., Shaul, Y., Schreiber, G. & Herrmann, C. (2004). Electrostatically optimized Ras-binding Ral guanine dissociation stimulator mutants increase the rate of association by stabilizing the encounter complex. *Proc. Natl Acad. Sci. USA*, **101**, 9223–9228.
15. Nocek, J. M., Zhou, J. S., de Forest, S., Priyadarshy, S., Beratan, D. N., Onuchic, J. N. & Hoffman, B. M. (1996). Theory and practice of electron transfer within protein–protein complexes: application to multidomain binding of cytochrome *c* by cytochrome *c* peroxidase. *Chem. Rev.* **96**, 2459–2490.
16. Erman, J. E. & Vitello, L. B. (2002). Yeast cytochrome *c* peroxidase: mechanistic studies via protein engineering. *Biochim. Biophys. Acta*, **1597**, 193–220.
17. Pelletier, H. & Kraut, J. (1992). Crystal structure of a complex between electron transfer partners, cytochrome *c* peroxidase and cytochrome *c*. *Science*, **258**, 1748–1755.
18. Volkov, A. N., Worrall, J. A. R., Holtzmann, E. & Ubbink, M. (2006). Solution structure and dynamics of the complex between cytochrome *c* and cytochrome *c* peroxidase determined by paramagnetic NMR. *Proc. Natl Acad. Sci. USA*, **103**, 18945–18950.
19. Worrall, J. A. R., Kolczak, U., Canters, G. W. & Ubbink, M. (2001). Interaction of yeast *iso*-1-cytochrome *c* with cytochrome *c* peroxidase investigated by [^{15}N,^{1}H] heteronuclear NMR spectroscopy. *Biochemistry*, **40**, 7069–7076.
20. Nakani, S., Viriyakul, T., Mitchell, R., Vitello, L. B. & Erman, J. E. (2006). Characterization of a covalently linked yeast cytochrome *c*–cytochrome *c* peroxidase complex: evidence for a single, catalytically active cytochrome *c* binding site on cytochrome *c* peroxidase. *Biochemistry*, **45**, 9887–9893.
21. Pearl, N. M., Jacobson, T., Arisa, M., Vitello, L. B. & Erman, J. E. (2007). Effect of single-site charge-reversal mutations on the catalytic properties of yeast cytochrome *c* peroxidase: mutations near the high-affinity cytochrome *c* binding site. *Biochemistry*, **46**, 8263–8272.
22. Pearl, N. M., Jacobson, T., Meyen, C., Clementz, A. G., Ok, E. Y., Choi, E. *et al.* (2008). Effect of single-site charge-reversal mutations on the catalytic properties of yeast cytochrome *c* peroxidase: evidence for a single, catalytically active, cytochrome *c* binding domain. *Biochemistry*, **47**, 2766–2775.
23. Sobolev, V., Sorokine, A., Prilusky, J., Abola, E. E. & Edelman, M. (1999). Automated analysis of interatomic contacts in proteins. *Bioinformatics*, **15**, 327–332.
24. Erman, J. E., Kresheck, G. C., Vitello, L. B. & Miller, M. A. (1997). Cytochrome *c*/cytochrome *c* peroxidase complex: effect of binding-site mutations on the thermodynamics of complex formation. *Biochemistry*, **36**, 4054–4060.
25. Pielak, G. J. & Wang, X. (2001). Interactions between yeast *iso*-1-cytochrome *c* and its peroxidase. *Biochemistry*, **40**, 422–428.
26. Reichmann, D., Rahat, O., Albeck, S., Meged, R., Dym, O. & Schreiber, G. (2005). The modular architecture of protein–protein binding interfaces. *Proc. Natl Acad. Sci. USA*, **102**, 57–62.
27. Schreiber, G. & Fersht, A. R. (1995). Energetics of protein–protein interactions: analysis of the barnase–barstar interface by single mutations and double mutant cycles. *J. Mol. Biol.* **248**, 478–486.
28. Frisch, C., Schreiber, G., Johnson, C. & Fersht, A. R. (1997). Thermodynamics of the interaction of barnase and barstar: changes in free energy *versus* changes in enthalpy on mutation. *J. Mol. Biol.* **267**, 696–706.
29. Harel, M., Cohen, M. & Schreiber, G. (2007). On the dynamic nature of the transition state for protein–protein association as determined by double-mutant

cycle analysis and simulation. *J. Mol. Biol.* **371**, 180–196.
30. Zuiderweg, E. R. P. (2002). Mapping protein–protein interactions in solution by NMR spectroscopy. *Biochemistry*, **41**, 1–7.
31. Prudêncio, M. & Ubbink, M. (2004). Transient complexes of redox proteins: structural and dynamic details from NMR studies. *J. Mol. Recognit.* **17**, 524–539.
32. Worrall, J. A. R., Liu, Y., Crowley, P. B., Nocek, J. M., Hoffman, B. M. & Ubbink, M. (2002). Myoglobin and cytochrome b_5: a nuclear magnetic resonance study of a highly dynamic protein complex. *Biochemistry*, **41**, 11721–11730.
33. Worrall, J. A. R., Reinle, W., Bernhardt, R. & Ubbink, M. (2003). Transient protein interactions studied by NMR spectroscopy: the case of cytochrome *c* and adrenodoxin. *Biochemistry*, **42**, 7068–7076.
34. Volkov, A. N., Ferrari, D., Worrall, J. A. R., Bonvin, A. M. J. J. & Ubbink, M. (2005). The orientations of cytochrome *c* in the highly dynamic complex with cytochrome b_5 visualized by NMR and docking using HADDOCK. *Protein Sci.* **14**, 799–811.
35. Xu, X., Reinle, W., Hannemann, F., Konarev, P. V., Svergun, D. I., Bernhardt, R. & Ubbink, M. (2008). Dynamics in a pure encounter complex of two proteins studied by solution scattering and paramagnetic NMR spectroscopy. *J. Am. Chem. Soc.* **130**, 6395–6403.
36. Kraulis, P. J. (1991). MOLSCRIPT: a program to produce both detailed and schematic plots of protein structures. *J. Appl. Crystallogr.* **24**, 946–950.
37. Merritt, E. A. & Bacon, D. J. (1997). Raster3D: photorealistic molecular graphics. *Methods Enzymol.* **277**, 505–524.
38. Rajamani, D., Thiel, S., Vajda, S. & Camacho, C. J. (2004). Anchor residues in protein–protein interactions. *Proc. Natl Acad. Sci. USA*, **101**, 11287–11292.
39. Clore, G. M., Tang, C. & Iwahara, J. (2007). Elucidating transient macromolecular interactions using paramagnetic relaxation enhancement. *Curr. Opin. Struct. Biol.* **17**, 603–616.
40. Solmaz, S. R. N. & Hunte, C. (2008). Structure of complex III with bound cytochrome *c* in reduced state and definition of a minimal core interface for electron transfer. *J. Biol. Chem.* **283**, 17542–17549.
41. Reichmann, D., Phillip, Y., Carmi, A. & Schreiber, G. (2008). On the contribution of water-mediated interactions to protein-complex stability. *Biochemistry*, **47**, 1051–1060.
42. Janin, J. (1999). Wet and dry interfaces: the role of solvent in protein–protein and protein–DNA recognition. *Structure*, **7**, R277–R279.
43. Rodier, F., Bahadur, R. P., Chakrabarti, P. & Janin, J. (2005). Hydration of protein–protein interfaces. *Proteins*, **60**, 36–45.
44. Kortemme, T. & Baker, D. (2002). A simple physical model for binding energy hot spots in protein–protein complexes. *Proc. Natl Acad. Sci. USA*, **99**, 14116–14121.
45. Kortemme, T., Kim, D. E. & Baker, D. (2004). Computational alanine scanning of protein–protein interfaces. *Sci. STKE*, **2004**, pl2.
46. Ofran, Y. & Rost, B. (2007). Protein–protein interaction hotspots carved into sequences. *PLoS Comput. Biol.* **3**, e119.
47. Hubbard, S. J. & Thornton, J. M. (1993). NACCESS Department of Biochemistry and Molecular Biology, University College London, London, UK; http://www.bioinf.manchester.ac.uk/naccess/.
48. Pollock, W. B. R., Rosell, F. I., Twitchett, M. B., Dumont, M. E. & Mauk, A. G. (1998). Bacterial expression of a mitochondrial cytochrome *c*. Trimethylation of Lys 72 in yeast *iso*-1-cytochrome *c* and the alkaline conformational transition. *Biochemistry*, **37**, 6124–6131.
49. Morar, A. S., Kakouras, D., Young, G. B., Boyd, J. & Pielak, G. J. (1999). Expression of ^{15}N-labeled eukaryotic cytochrome *c* in *Escherichia coli*. *J. Biol. Inorg. Chem.* **4**, 220–222.
50. Goodin, D. B., Davidson, M. G., Roe, J. A., Mauk, A. G. & Smith, M. (1991). Amino acid substitutions at tryptophan-51 of cytochrome *c* peroxidase: effects on coordination, species preference for cytochrome *c*, and electron transfer. *Biochemistry*, **30**, 4953–4962.
51. Piotto, M., Saudek, V. & Sklenár, V. (1992). Gradient-tailored excitation for single-quantum NMR spectroscopy of aqueous solutions. *J. Biomol. NMR*, **2**, 661–665.
52. Helgstrand, M., Kraulis, P. J., Allard, P. & Hard, T. (2000). Ansig for Windows: an interactive computer program for semiautomatic assignment of protein NMR spectra. *J. Biol. NMR*, **18**, 329–336.
53. Mauk, M. R., Ferrer, J. C. & Mauk, A. G. (1994). Proton linkage in formation of the cytochrome *c*–cytochrome *c* peroxidase complex: electrostatic properties of the high- and low-affinity cytochrome *b*inding sites on the peroxidase. *Biochemistry*, **33**, 12609–12614.
54. Wiseman, T., Williston, S., Brandts, J. F. & Lin, L. N. (1989). Rapid measurement of binding constants and heats of binding using a new titration calorimeter. *Anal. Biochem.* **179**, 131–137.
55. Case, D. A. (1995). Calibration of ring-current effects in proteins and nucleic acids. *J. Biomol. NMR*, **6**, 341–346.
56. Haigh, C. W. & Mallion, R. B. (1979). Ring current theories in nuclear magnetic resonance. *Prog. NMR. Spectrosc.* **13**, 303–344.
57. Schwieters, C. D., Kuszewski, J. J., Tjandra, N. & Clore, G. M. (2003). The Xplor-NIH NMR molecular structure determination package. *J. Magn. Reson.* **160**, 66–74.